Chapter 5

The Luminous Infrared Merger:– NGC 6240

5.1 Introduction

Interactions and mergers of gas-rich galaxies are important in the triggering of starbursts (Larson & Tinsley 1978; Barnes & Hernquist 1996) and nuclear activity (Norman & Scoville 1988). Starburst activity comprises of an intense, short-lived period of star-formation, often associated with spectra dominated by emission in the infrared due to dust heated by UV emission from hot, young stars (Rieke et al. 1985; Shier, Rieke & Rieke 1996). As a consequence many luminous and ultra luminous infrared galaxies (ULIRGs, $L_{(8-1000\mu m)} > 10^{12}L_{\odot}$ Sanders et al. 1988) are also classified as starbursts and a significant fraction (12 to 25%) are known to be interacting systems (Soifer et al. 1984). Activity in galaxies such as Seyferts and quasars manifests itself as a compact AGN. The infrared luminosities observed in ULIRGs could also be attributed to a hidden AGN heating surrounding obscuring dust (Genzel et al. 1998; Sanders et al. 1988). A dynamical and spatial study of the neutral gas component on sub-

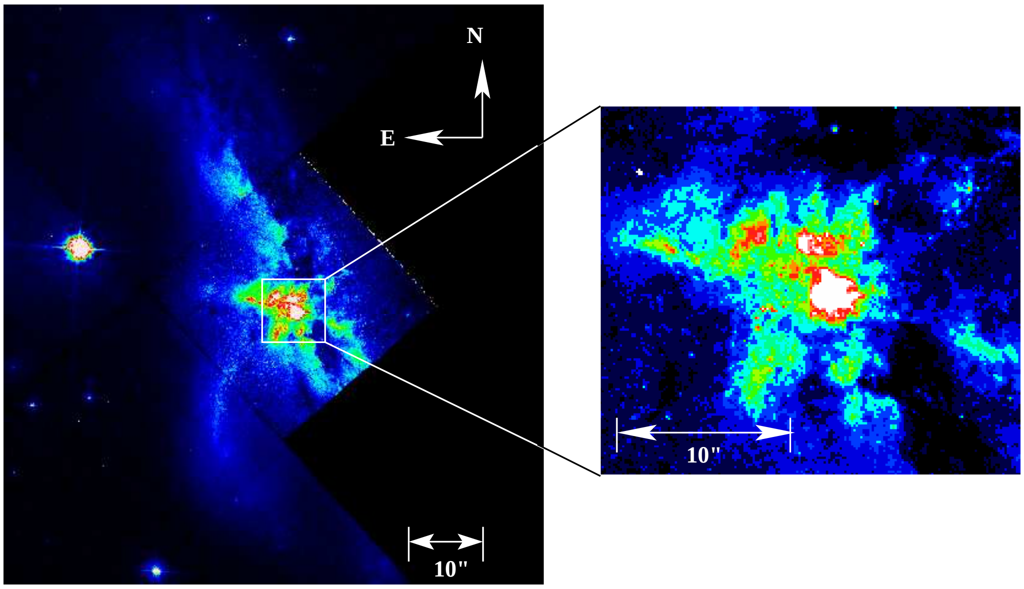

Figure 5.1: An archival *HST* WFPC-2 (filter: F814W) image of the central region of the luminous infrared merger NGC 6240. The inset shows an enlarged view of the central region of the merger show two optical nuclei and heavy associated optical obscuration.

arcsecond scales is essential to gain a broader understanding of such disrupted galaxies. The resolution of MERLIN can be used to observe neutral hydrogen (H I) in absorption on ∼0.1 arcsecond scales, corresponding to tens of parsecs in the nearest ULIRGs (e.g. Cole et al. 1998b) making it the ideal instrument for such a study.

5.1.1 Background – NGC 6240

NGC 6240 (D=97 Mpc for H_0=75 km s^{-1}Mpc^{-1}; $1''$=470 pc) is a prototypical luminous infrared merger ($L_{bol} \sim L_{fir} = L_{8-1000\mu m} = 6 \times 10^{11}\,L_\odot$, Sanders et al. 1988) with an extremely complex morphology. The central region harbors two compact sources separated by $\sim 1\farcs5$ (700 pc). In the optical (see Fig. 5.1) an extensively distorted system is observed with tidal tails (Fosbury & Wall 1979;

Fried & Schulz 1983) consistent with interaction remnants of the type discussed by Toomre & Toomre (1972). NGC 6240 is accepted by many to be undergoing a major starburst of Arp 220 proportions, although maybe at an earlier stage (Tacconi et al. 1999), with strong CO 2.3μm absorption and near infrared imaging and spectroscopic detections (Tecza et al. 2000; Ohyama et al. 2000). In addition NGC 6240 also demonstrates many qualities associated with AGN, such as two compact cores (Carral, Turner & Ho 1990), an optical spectrum that is somewhere between that of a Seyfert-2 and LINER (Armus, Heckman & Miley 1990; Heckman et al. 1987; Depoy, Becklin & Wynn-Williams 1986) and the detection of a strong iron-K emission line (Tanaka, Inoue & Holt 1994; Ikebe et al. 2000). Recent high resolution *Chandra* observations of NGC 6240 (Lira et al. 2002) directly detect the two nuclei and an area of complex extended X-ray emission. It is clear that strong star-formation is occurring in NGC 6240, although it is still in debate as to whether or not some of the galaxy's activity is due to more 'classical' AGN activity.

Continuum radio frequency observations of NGC 6240, such as those by Colbert, Wilson & Bland-Hawthorn (1994), Carral et al. (1990) and Eales et al. (1990) have achieved the resolution required to begin to image the continuum structure of the two compact cores, but with no dynamical information. Early spectral line observations by Baan et al. (1985) and Dickey (1982) revealed both broad HI and OH absorption but these observations had insufficient spatial resolution to make a detailed study of the gas structure within the central region of NGC 6240. Additionally recent monitoring of this source with the single dish radio telescopes has also detected weak H_2O maser emission from the direction NGC 6240 (Hagiwara et al. 2002; Nakai et al. 2002). This detected maser emission is redshifted by $\sim$260$\rightarrow$300 km s^{-1} with respected to the systemic velocity of the galaxy and has a large maser luminosity of $\sim$40 L$_\odot$. It is concluded that this maser emission may originate from near to an AGN, possibly within a rotating maser disc resulting in high velocities relative to the systemic velocity, although the position of the water maser emission is still undetermined relative to the previously observed radio emission.

In this chapter sub-arcsecond angular resolution observations of HI absorption made with MERLIN against the core and intermediate scale radio continuum within the central region of NGC 6240 are presented. These observations represent the highest angular resolution dynamical study of the neutral hydrogen distribution within the centre of this merging galaxy to be made to date. In addition three epochs of 5 GHz MERLIN observations of NGC 6240, with $\sim 0\farcs1$ resolution are presented.

5.2 Observations and Image Processing

NGC 6240 was observed at 20 cm with the MERLIN array using 7 telescopes, including the Lovell telescope, with a maximum baseline of 217 km (Thomasson 1986) on January 31st 1996. Opposite hands of circular polarisations were measured with 8-MHz bandwidths and correlated into 64 channels each of a bandwidth of 125-kHz (26.3 km s^{-1}). The frequency of channel 32 was observed at the velocity of NGC 6240 (7300 km s^{-1}).

Eleven hours of observations of NGC 6240 were taken, interspersed regularly with observations of the phase calibrator (1648+015) and a bandpass calibrator (0552+398). The flux density scale was determined from an observation of 3C 286, which was assumed to have a flux density of 15.0 Jy (Baars et al. 1977). Preliminary flux calibration and gain-elevation corrections were applied to the data using local MERLIN software, before transferring the data into AIPS.

A bandpass calibration, phase corrections and additional editing of the data were achieved using set tasks within AIPS. The resulting data were Fourier transformed using HORUS producing $512 \times 512 \times 64$ spectral line cubes, weighted both naturally

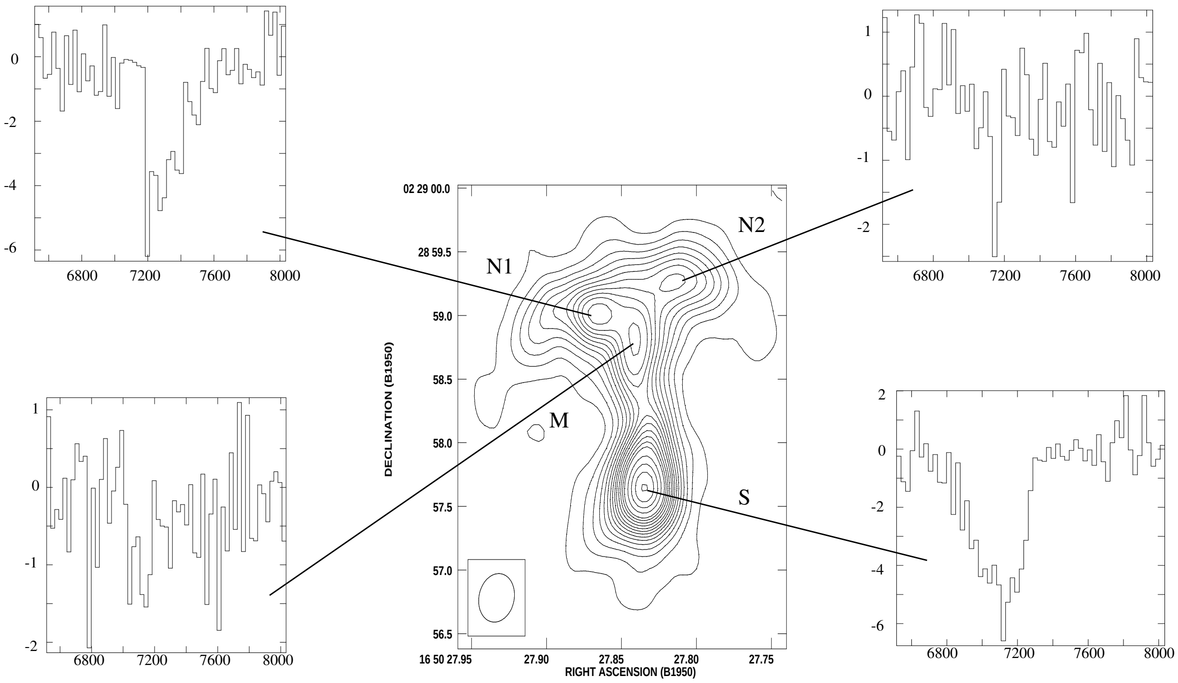

Figure 5.2: A montage showing a 1.4 GHz naturally weighted continuum map of the central area of NGC 6240 with selected absorption spectra supposed. The angular resolution of the image is $0\farcs394 \times 0\farcs343$ and contour levels are set at -2, 2, 4, 6, 8, 10, 12, 14, 16, 18, 20, 22.5, 25, 27.5, 30, 35, 40, 45 and 50 mJy beam^{-1}. The spectra are plotted with flux density in mJy beam^{-1} against velocity in km s^{-1}.

and uniformly. Twenty channels (channels 6-15, 53-62) free from absorption were combined to create continuum maps, which were subsequently used to produce naturally and uniformly weighted continuum-subtracted spectral cubes. The telescope beam was deconvolved using the AIPS task APCLN which utilises the CLEAN deconvolution algorithm (Högbom 1974). The cleaned continuum images were added back to the continuum subtracted cubes and analysed using the standard AIPS tasks. The tapering (300 kλ) of these data produced images which were also sensitive to some large, diffuse regions of emission towards the west and south of the central kiloparsec which are not presented here. The contributions to self-calibration models of this component were found to be minimal ($\lesssim$10%) and hence were ignored.

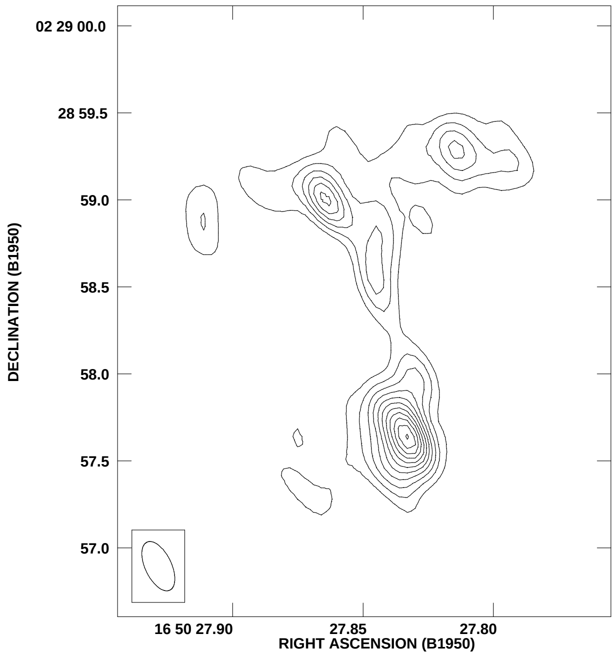

Figure 5.3: 1.4 GHz uniformly weighted continuum map of the central NGC 6240 with a resolution of 0.305× 0.151 arcsec. The contour levels are set at -2, 2, 3, 4, 5, 6, 7, 8, 9, 10, 11 and 12 mJy beam^{-1}.

In addition to 1.4 GHz spectral line data, a 5 GHz MERLIN continuum image was formed in a similar manner from 10 hours of observations taken on January 12th 1998. This data set also contained two 8-MHz bands of opposite circular polarisation and were correlated in 64 channels centred on 4.72 GHz, the redshifted H_2CO line, to search for absorption. Unfortunately no H_2CO absorption was found at the sensitivity achieved but this did enable a high resolution continuum map to be made. The data was used to derive limits upon the optical depths of H_2CO in front of the two main radio sources by placing a detection level limit of five times the rms error on these spectra. The resulting limits for the optical depths are southern source $\tau(H_2CO)\leq 0.1$ and northern source $\tau(H_2CO)\leq 0.2$. To complement this two additional 5 GHz MERLIN radio continuum observations of NGC 6240 are also presented

5.3 Results

5.3.1 Continuum Observations

Naturally and uniformly weighted 1.4 GHz continuum images of NGC 6240 are shown in Figs. 5.2 & 5.3. The angular resolution of the uniform weighted image is $0''.31 \times 0''.15$ with a noise level of 0.20 mJy beam^{-1} and the naturally weighted map has resolution of $0''.39 \times 0''.34$ with a noise level of 0.16 mJy beam^{-1}. The resolution of the images is reduced due to the poor UV coverage achieved with MERLIN for low declination sources such as NGC 6240 ($\delta \approx 2^{\circ}$). This also results in some elongation of the telescope beam. The continuum results are consistent with previously published 3.6 cm VLA images of Colbert et al. (1994). They show clearly resolved northern and southern components along with a third peak visible alongside the northern component. In addition the 1.4 GHz image also shows a component between S and N1 not seen in Colbert et al.'s images. Fig. 5.4 shows a contour map at 5 GHz with a resolution of $0''.102 \times 0''.055$ and a noise level of 0.1 mJy beam^{-1}. This map shows the two compact radio sources seen by Carral et al. (1990). The slightly extended nature of the southern component is likely to be the result of the elliptical beam-shape achieved with MERLIN at this declination. The flux densities of these two components, along with those of other features seen in the maps at both 1.4 and 5 GHz, are given in Table 5.1 with additional flux densities from the literature and calculated spectral indices. The spectral index α is defined as $S_{\nu} \propto \nu^{-\alpha}$ and was calculated between each frequency. The value of α displayed in Table 5.1 is a mean of all of the possible calculated values from the frequency pairs, shown in Table 5.1. The uncertainties given in Table 5.1 are a result of variations in background emission between different resolution images. Limits on the spectral index are given for component M (see Fig. 5.2) based upon a non-detection at five times the rms noise level of the 5 GHz image.

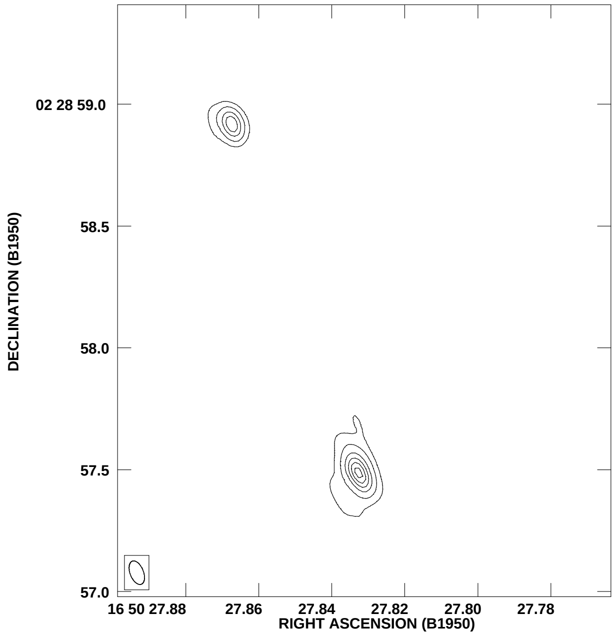

Figure 5.4: 5 GHz naturally weighted continuum map of NGC 6240 with a resolution of $0.102\times0.055\,\mathrm{arcsec}^2$. The contour levels are set at -2, 2, 5, 10, 15, 20 and 25 $\times0.5\,\mathrm{mJy\,beam}^{-1}$.

5.3.2 Spectral Line Data

The HI absorption data were formed into both uniform and naturally weighted cubes. In both, absorption is seen against the two dominant nuclei. The noise levels of the two cubes were $0.20\,\mathrm{mJy\,beam}^{-1}$ and $0.16\,\mathrm{mJy\,beam}^{-1}$ respectively. Some additional, weaker, absorption was also observed in the naturally weighted cube against the components N2 (west of the main northern nucleus) and M (between the two main components). Single channel contour maps of the continuum-subtracted naturally weighted cube are shown in Fig. 5.5. Absorption can be seen over 19 channels, with the absorption against both cores clearly centred at different velocities, as can also be seen in the spectra displayed in Fig. 5.2.

Three position-velocity (p-v) plots were also formed by averaging 0.32 arcsecond wide strips along the position angle of the two dominant components. These

Component	R.A. (B1950) 16^h50^m	Dec. (B1950) $02°28'$	$S_{1.4GHz}$ mJy	S_{5GHz} mJy	$S_{8.4GHz}$ mJy	S_{15GHz} mJy	Spectral Index α
S	$27^s.83$	$57''.5$	65.1	36.8	31±2	14.7±2	0.66
N1	27.86	58.9	30.4	16.1	14.4±0.7	5.9±1	0.71
M	27.84	58.8	15.3	-	-	-	≥ 1.1
N2	27.82	59.2	12.2	-	3.2±0.6	-	0.75

Table 5.1: Continuum properties of the strongest radio components in NGC 6240 as detected at 1.4 GHz, 5 GHz, 8.4 GHz and 15 GHz. The 8.4 GHz and 15 GHz flux densities were taken from Colbert et al. (1994) and Carral et al. (1990).

are shown in Fig. 5.6, where Fig. 5.6b represents a slice through the centre of the components, whilst Fig. 5.6a and 5.6c are slices showing the velocity structure 0.32 arcseconds northwest and southeast of the central slice. Fig. 5.7 shows the velocity gradients across each of the two core components where absorption was detected.

Summarised in Table 5.2 are the neutral hydrogen absorption properties of NGC 6240. The component labels are listed in column 1 and correspond to the same components referred to in Table 5.1 and Fig. 5.2. Their peak optical depth, $\int \tau \, dV$ and the radial velocities of the absorption lines, determined from Gaussian fitting to the spectra, are listed in columns 2, 3 and 4. Column 5 is the column density, calculated using $N_H = 1.823 \times 10^{20} \int \tau \, dV$, assuming an electron spin temperature of 100 K.

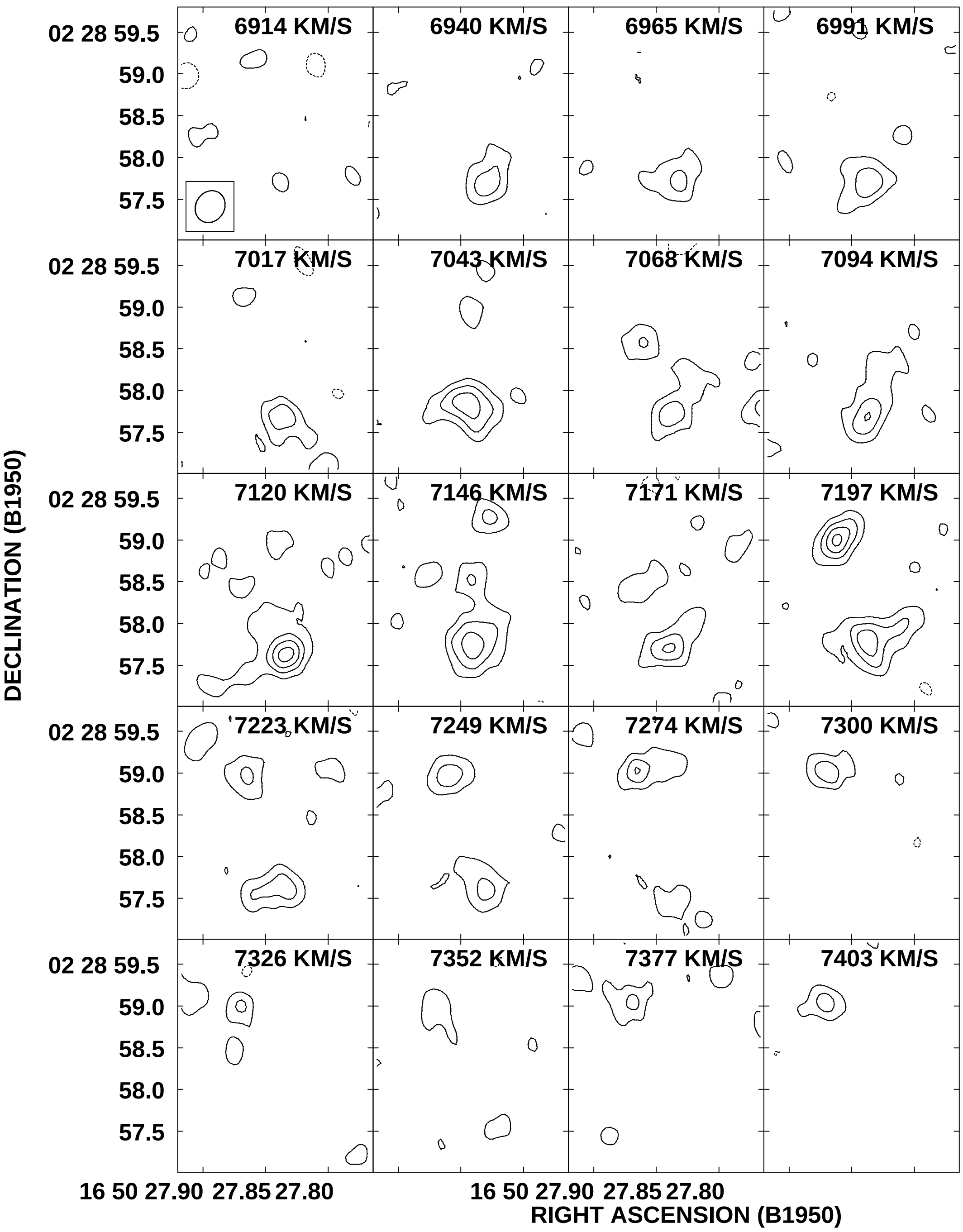

Figure 5.5: Contour maps of the naturally weighted continuum-subtracted spectral line cube for 20 frequency channels over which absorption is present. The contours shown are -6, -5, -4, -3, -2, -1 and 1 $\times 1.7\,\mathrm{mJy\,beam^{-1}}$. The central velocity of each map is given in $\mathrm{km\,s^{-1}}$.

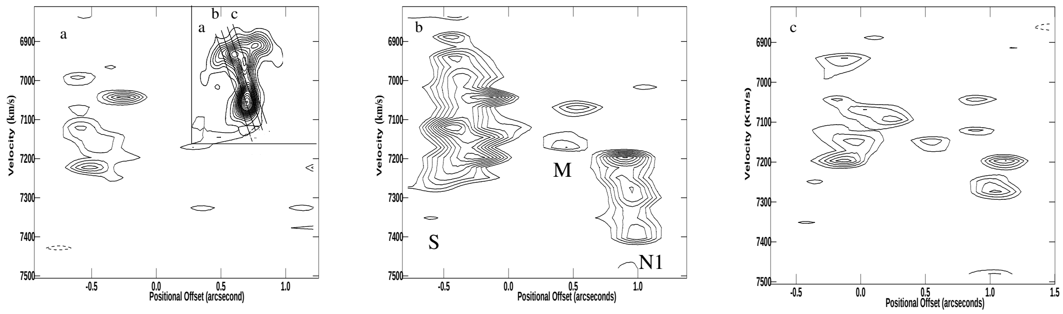

Figure 5.6: The mean position-velocity plots obtained by averaging the naturally weighted continuum-subtracted cube over a strip 0.32 arcsecond wide oriented at an angle of +20° from the vertical, bisecting components N1 and S. The positive positional offset corresponds to north-east of reference position (16^{h} 50^{m} $27^{s}.80$, 02° 28′ 58″.0). The contour levels are -6, -5.5, -5, -4.5, -4, -3.5, -3, -2.5, -2, -1.5 and 1.5 mJy beam^{-1}. The continuum map inset into the left hand image shows the positions over which the three position-velocity plots are averaged.

5.4 Discussion

5.4.1 Continuum

The 1.4 GHz continuum image (Fig. 5.2) shows the several distinct components, in particular two cores (N1 and S) along with two weaker clumps of emission, N2 lying west of N1, and M a minor peak in emission between the two compact cores. This structure is consistent with the morphology reported by Colbert et al. (1994) in his 3.6 cm VLA A-configuration maps, although Colbert et al. do not detect component M. In the uniformly weighted map the components N2 and M become even more apparent (see Fig. 5.3). Regions of diffuse, lower surface brightness, to the west and south of the central kiloparsec of the galaxy seen in Colbert et al.'s 20 cm continuum image (beyond the extent of the continuum image shown here) were also detected in the naturally weighted absorption-free channels.

The two compact cores (S and N1) are unresolved in the 5 GHz MERLIN image, with only some extended structure in the southern component. Carral et al. (1990) found comparable structure in their 15 GHz VLA image, which has similar angular resolution to the 5 GHz MERLIN image shown in Fig. 5.4. The separation of these two cores is 1.52 ± 0.01 arcsec ($\sim$715 pc) in both the 1.4 and 5 GHz maps agreeing with the $1''.5$ recorded by Colbert et al. No emission is detected at the positions of either N2 or M at 5 GHz, either a result of MERLIN at 5 GHz not being sensitive to diffuse emission or an indication that these components have steeper spectral indices than S and N1. For component M, limits on its spectral index were calculated using a minimum detection level at 5 GHz of five times the rms noise level (see Table 5.2). As can be seen from Table 5.2 the spectral indices of S & N1 are relatively flat ($\alpha \approx 0.6 \rightarrow 0.7$), whereas for M, the calculated limit is $\alpha \geq 1.1$.

5.4.2 Spectral Line Mapping

Broad HI absorption is observed against S and N1 as seen in the spectra displayed in Fig. 5.2. This broad absorption is evident in previous single dish spectral line observations (Baan et al. 1985; Heckman et al. 1985) which also show systemic velocities consistent with those presented here. The two core components clearly show broad absorption at different velocities. In Fig. 5.5 these broad absorption peaks are easily seen, centred at $\sim$7100 and 7250 km s^{-1} for the southern and northern components respectively. The velocity difference between the peaks measured from these data is confirmed by results of stellar CO absorption observations of similar spatial resolution which find the northern core redshifted relative to the southern nucleus by 137 and 147 km s^{-1} Tecza et al. (2000) and Freid & Ulrich (1985) respectively. In general the absorption structure is dominated by the two compact cores each with complex velocity components. Fig. 5.6b shows a $0''.32$ cut through the centre of these two compact components. Five distinct absorption components are visible within S spanning a velocity range of $\sim$400 km s^{-1}. The northern core, N1, shows three velocity components spread

Component	$\tau_{\rm peak}$	V_c ($\rm km\,s^{-1}$)	$\int \tau dV$ ($\rm km\,s^{-1}$)	N_H ($\times 10^{21}\rm cm^{-2}$)
S	0.15	7087	82.8	15.1
N1	0.31	7260	114.1	20.8
M	0.09	-	$\leq$24.7	$\leq$4.5
N2	0.12	-	$\leq$9.47	$\leq$1.73

Table 5.2: A summary of neutral hydrogen absorption properties of NGC 6240.

over the range 7200$\rightarrow$7425 $\rm km\,s^{-1}$. The large overall velocity range is consistent with single dish HI absorption observations (Baan et al. 1985) and previous interferometer spectra taken by Dickey (1982). Each of the four components have optical depths ranging between, ~0.1 and 0.3. The similarity in optical depths suggests that the gas disc uniformly covers the nuclear region. The non-detection of broad absorption against N1 and M result from either a positional effect (i.e. the continuum source is between us and the gas) or from the background source not being sufficiently bright for the absorption to be detected.

5.5 Origins of the Radio Emission

The morphology of the nuclear region in NGC 6240 is consistent with the merging of two galaxies with compact nuclei observed as compact radio sources, however the energy source for the radio frequency emission is less easily described. NGC 6240 is a strong far-infrared emitter, with a high luminosity, making it difficult to classify as either starburst or Seyfert (Carral et al. 1990).

In the following section the possible origin for the radio emission observed in NGC 6240 will be discussed. Flux densities will be considered along with the observed spatial structure and used to evaluate the plausibility of a purely starburst energy source, an AGN or a combination of these producing the observations presented here.

5.5.1 All Radio Emission due to Starburst Activity

From the general shape, size ($\sim 700 \times 500$ pc) and structure of the nuclear region of NGC 6240 seen in the low resolution 1.4 GHz map it could be argued that the emission is purely a result of starburst activity triggered by the interaction of two gas rich galaxies. This starburst emission would thus be the result of relativistic charged particles accelerated in supernovae remnants (SNRs) and radio supernovae (RSNe) similar to those in M82 (Muxlow et al. 1999) and other starburst galaxies.

The prototypical luminous infrared starburst galaxy merger Arp 220 (distance 75 Mpc) is often closely compared to NGC 6240 (distance 97 Mpc), since they have many similar characteristics. VLBI observations of Arp 220 have detected a number of compact millijansky luminous radio supernovae at 18 cm within the nuclear region (Smith et al. 1998a). If it is assumed that the central region of NGC 6240 contains similar point sources originating from a starburst; can we feasibly account for the observed 20 cm flux densities of the nuclear region? From these observations the 20 cm continuum flux densities of S (65 mJy) and N1 (30 mJy) would require $\sim$100 and 50 RSNe of a similar luminosity to the youngest, brightest RSN found in Arp 220. This number of sources could be present in such an actively merging galaxy as NGC 6240, especially if it is considered that in galaxies such as Arp 220 and M82 not all of the radio continuum originates in RSNe. Hence the required numbers can be reduced to more modest levels. The possibility of such a scenario is reinforced by recent VLBA observations that may have detected a millijansky RSN $\sim$0$''\!\!.$25 north of the southern nucleus (Gallimore private communication).

The other main considerations are the star-formation and supernova rates re-

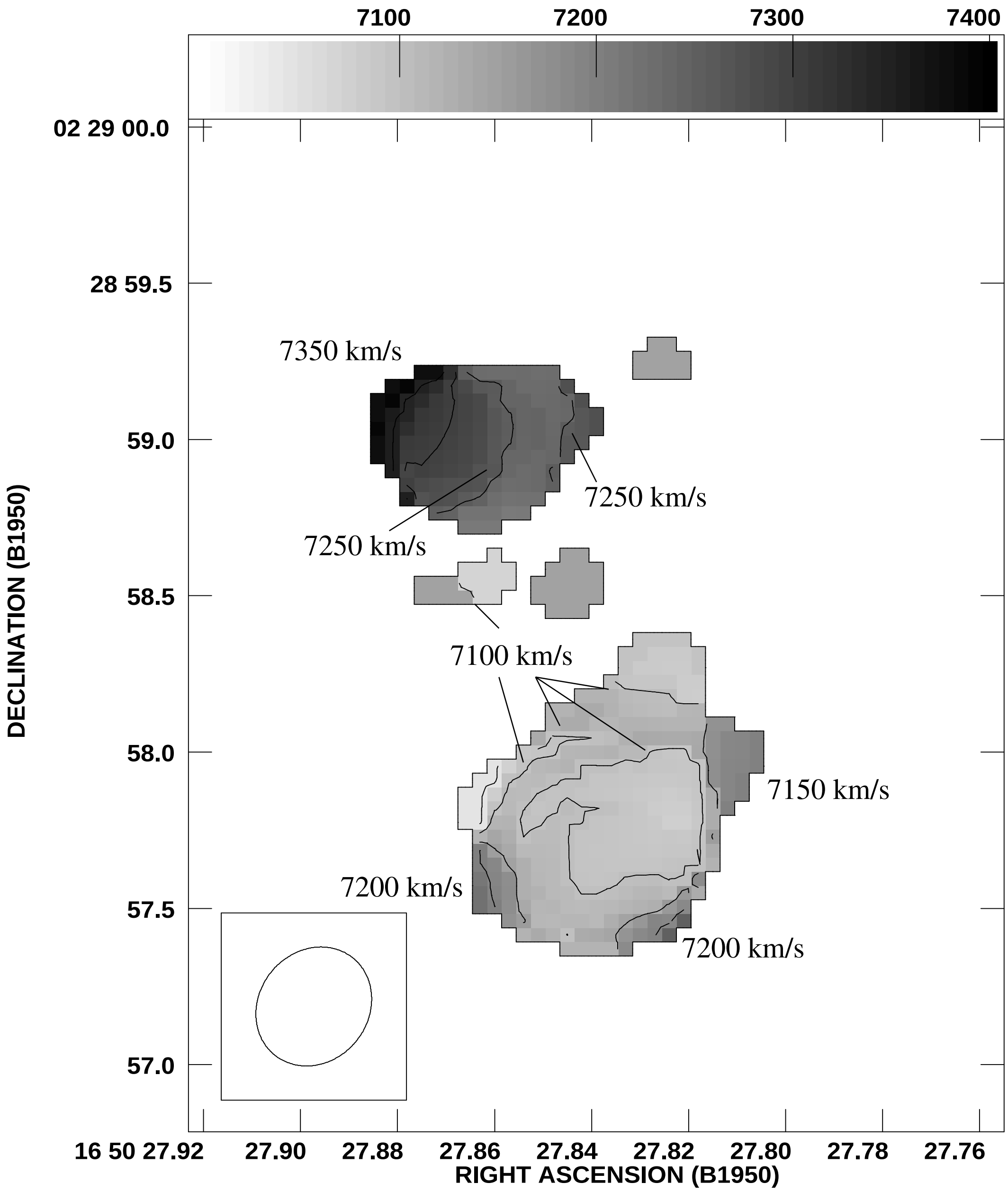

Figure 5.7: The velocity gradient of the absorbing gas across the two compact components. The contours are at $50\,\mathrm{km\,s^{-1}}$ intervals between 7050 and $7350\,\mathrm{km\,s^{-1}}$ with the grey scale ranging from $7000 \rightarrow 7400\,\mathrm{km\,s^{-1}}$.

quired to achieve this high number of observed supernovae. Cram et al. (1998) showed that the radio luminosity from star forming galaxies can be considered as directly proportional to the supernovae rate in the galaxy, since the radio luminosity is not significantly affected by extinction. Using this, a star-formation rate (SFR) can be estimated with an initial mass function tailored to yield stars, massive enough to form supernovae that produce significant radio emission ($\geq$8 $M_\odot$). This can be derived from the 1.4 GHz luminosity (Cram et al. 1998) as follows:

$$\mathrm{SFR}_{1.4}(\mathrm{M} \geq 1\mathrm{M}_\odot) = \frac{L_{1.4}}{1.66 \times 10^{21}\mathrm{WHz}^{-1}}\mathrm{M}_\odot\mathrm{yr}^{-1}. \tag{5.1}$$

From the above formula and the luminosities derived from these results, I find that for the whole of the nuclear region of NGC 6240 ($\mathrm{L}_{1.4}$ = 123 mJy) the $\mathrm{SFR}_{1.4}(\mathrm{M} \geq 1\mathrm{M}_\odot) = 83.1\mathrm{M}_\odot\,\mathrm{yr}^{-1}$. This value is comparable with the SFR calculated from the radio emission of Arp 220 of 109 $\mathrm{M}_\odot\,\mathrm{yr}^{-1}$, calculated with the same initial mass function (Smith et al. 1998a).

Using the Salpeter initial mass function, $\psi(m)$, (Salpeter 1955), the supernova rate, ν_{sn} can be calculated from,

$$\nu_{sn} = \mathrm{SFR}\frac{\int_{m_{sn}}^{m_u}\psi(m)dm}{\int_{m_l}^{m_u}\psi(m)mdm} \approx \frac{\mathrm{SFR}}{3}\frac{(m_{sn}^{-1.5} - m_u^{-1.5})}{(m_l^{-0.5} - m_u^{-0.5})}. \tag{5.2}$$

Assuming a lower mass limit of m_{sn}=8 $\mathrm{M}_\odot$ for a Type II supernova (with lower and upper mass limits of $m_l \approx 1\,\mathrm{M}_\odot$ and $m_u \approx 45\,\mathrm{M}_\odot$) the rate is calculated to be ν_{sn}=1.33 yr^{-1}. The supernova frequency of Arp 220 is ν_{sn}=1.75 yr^{-1} (Smith et al. 1998a). This supernova frequency calculated for NGC 6240 implies a new RSN could be expected to appear approximately every 9 months.

This scenario, although feasible is unlikely due to these flux density considerations and also because of the large number of sources which must be contained in the compact cores. Compact objects S and N1 are unresolved in the highest resolution maps presented here implying they have linear sizes of $\leq$ 26 pc. Emission peaks M and N2 have lower flux levels and are more extended making their emission more likely to be of starburst origin.

5.5.2 Active Galactic Nuclei

The two compact cores seen in Fig. 5.4 & 5.8 are unresolved, with radio flux densities larger than those expected from galaxies with starbursts alone. They also have spectral indices of $\sim$0.7 (see Table 5.1) which is compatible with AGN emission. At a low resolution (Fig. 5.2) the overall radio morphology seen could be interpreted as jet-like structures emerging from the two compact radio sources. In this scenario jets can be used to explain the observed weaker emission peaks, N1 and M, with associated AGN in the compact cores.

The idea that a merger event can trigger the fuelling of an AGN is widely accepted. If this is so, it is conceivable that a violent merger event such as seen in NGC 6240 could trigger the fuelling of AGN in both nuclei of the merging galaxies. The general idea of the presence of one or more AGN-type source in NGC 6240 is also supported by observations at other wavelengths such as detection of broad FeK line emission (Tanaka et al. 1994), an optical spectral classification as a Seyfert-2/LINER (Armus et al. 1990) and the recent detection of H_2O maser emission (Hagiwara et al. 2002; Nakai et al. 2002).

5.5.3 Combination of AGN and Starburst

The possibility of the co-existence of an AGN and a starburst in a galaxy has been previously accepted (Genzel et al. 1998) and observed (e.g. Seyfert NGC 1068, Gallimore et al. 1996). The actual source of the emission in NGC 6240 is likely to be a combination of SNRs and RSNe from a starburst and emission associated with AGN activity. It is not possible to rule out that S and N1 are made up of highly luminous RSNe from an intense starburst, although their compact nature and large flux densities make them more likely to be AGN powered synchrotron cores. The two other components, N2 and M, have flux densities and structures which are more consistent with starburst activity. The position of M, between the main nuclei, is consistent with a starburst triggered at the gas collision front between the merging galaxies (Taniguchi, Trentham & Shioya 1998). This is supported by the strong shocked H_2 line emission observed between S and N1 (Ohyama et al. 2000; Rieke et al. 1985). Component N2's structure and position could imply it is formed from a bent jet emerging from S, interacting with interstellar material and inducing some starburst activity. Alternatively it could be a superwind of relativistic electrons ejected from N1, as suggested by Colbert et al. (1994). This picture is comparable to the 'bubbles' of radio emission seen in Mrk 6, a Seyfert galaxy with associated starburst emission (Kukula et al. 1996). It is suggested that these result from hot gas associated with a starburst region, a picture which would also consistently explain the observed emission of N2 in NGC 6240.

At the present time no observations with a high enough angular resolution to discriminate between unresolved individual components, such as RSN, within S and N1 have been published. Recent VLBA 2.3 GHz observations made on August 15$^{\mathrm{th}}$ 1999 and April 24$^{\mathrm{th}}$ 2000 (Gallimore, private communication) may have detected a radio luminous supernova remnant $0\farcs26$ north and $0\farcs14$ east of S with a flux density initially observed to be $1.3\,\mathrm{mJy\,beam^{-1}}$ in the first epoch which dimmed to $0.5\,\mathrm{mJy\,beam^{-1}}$ by the following observation (Gallimore & Beswick 2000). The radio luminosity of this suspected supernova is comparable to the luminous RSNe detected in Arp 220 (Smith et al. 1998a).

In order to attempt to confirm the detection of an RSNe in NGC 6240 two

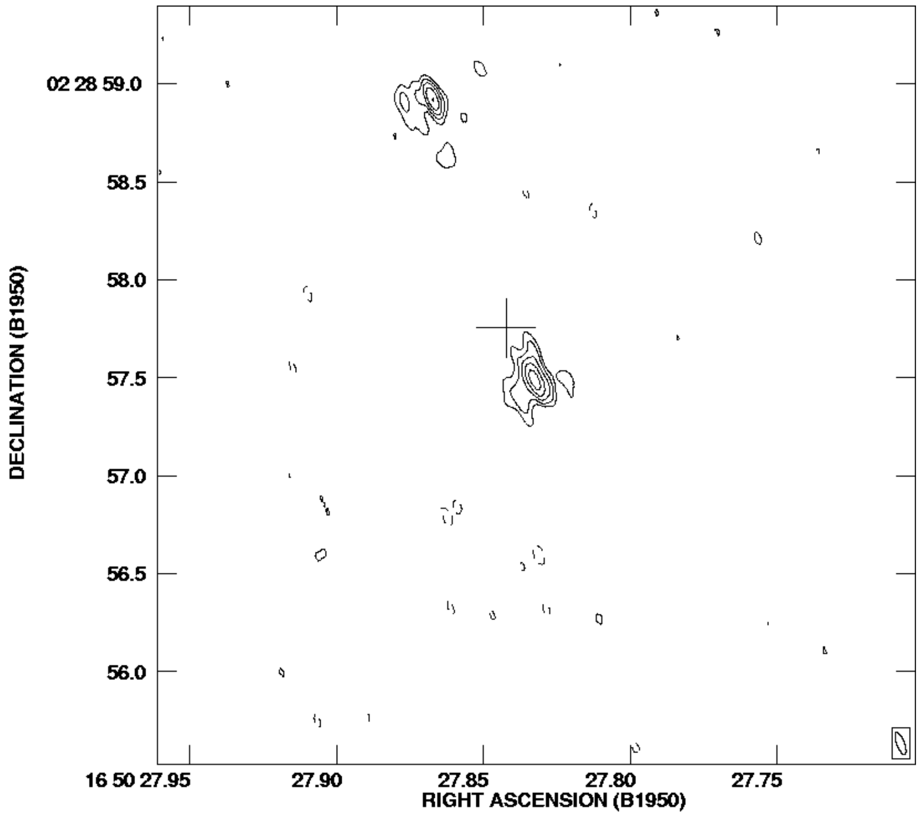

Figure 5.8: MERLIN 5 GHz continuum contour map of NGC 6240. The contour levels are -1, 1, 2, 4, 8, 16 $\times 455\mu$Jy beam^{-1}. The cross marks the reported position of a luminous RSN detected using the VLBA at 2.3 GHz (Gallimore, private communication).

full track MERLIN continuum observations at 5 GHz were granted from the MERLIN directors discretionary time. These were observed on May 18th and May 30th 2000. Fig. 5.8 shows a naturally weighted 5 GHz MERLIN contour map of NGC 6240 obtained on May 18$^{\rm th}$ 2000. The position marked on this image represents the reported position of the RSN. Although the reported RSN was not detected in either of these two observations, a limit upon its flux density of 500 μJy beam^{-1} at 5 GHz was set.

These two epochs of 5 GHz MERLIN observations, along with the previous 5 GHz observations (see Fig. 5.4) made on January 12$^{\rm th}$ 1998, have provided additional information about any flux densities variations of the two compact core-like com-

Component	12$^{\text{th}}$ January 1998	18$^{\text{th}}$ May 2000	30$^{\text{th}}$ May 2000
S	13.8 mJy bm^{-1}	11.2 mJy bm^{-1}	12.0 mJy bm^{-1}
N1	9.94 mJy bm^{-1}	7.62 mJy bm^{-1}	9.06 mJy bm^{-1}

Table 5.3: MERLIN peak flux density measurements of the compact components in NGC 6240 at 5 GHz over a 2 year period.

ponents in NGC 6240 (see Table 5.3). The flux densities of the two compact components, S and N1, are observed to vary by ~15% in these observations on a time-scale of ~2 years and by ~10→15% between the last two epochs (twelve days).

Wrobel (2000) has extensively monitored the continuum flux density of the nucleus of the Seyfert galaxy NGC 5548 at various wavelengths using the VLA and VLBA over a period of several years. The size of the radio flux variations in NGC 5548 that she found on time-scales of years are comparable to the variations that are found in the two compact components of NGC 6240 upon similar time-scales. Wrobel (2000) concluded that the variations seen in the nuclear flux density of NGC 5548 were consistent with a primary energy source of an AGN and inconsistent with compact star clustering models. This conclusion can only be considered as support for the hypothesis presented here that the majority of the radio flux emitted by the two compact components in NGC 6240 originates from a pair AGN rather than areas of densely spaced starburst activity.

5.6 Kinematics of NGC 6240

The two compact objects that are seen in the central region of NGC 6240 show distinctly differing central velocities split by 150 km s^{-1}. This velocity difference can been accounted for by considering them as two nuclei (see Fig. 5.9) associated with the original galaxies involved in the merger event (Tecza et al. 2000; Ohyama et al. 2000). This simplistic interpretation (Fig. 5.9) explains the velocity difference between the two primary component as due to the rotation of these two nuclei about each other. This is consistent with the measurements and interpretation of Tecza et al. (2000) and Ohyama et al. (2000).

The absorption spectra (see Fig. 5.2) are consistent with them being made up of at least two components, narrow and broad line absorption. The narrow line absorption component (FWHM$\sim 26 \rightarrow 52\,\mathrm{km\,s^{-1}}$) is apparent in spectra of N1, N2 and S. The centre of this component has a slight velocity shift between N1, N2 and S (N1: $7200\,\mathrm{km\,s^{-1}}$, N2: $7150\,\mathrm{km\,s^{-1}}$, S: $7125\,\mathrm{km\,s^{-1}}$). The dominant broader absorption component is also present in the spectra of S and N. This absorption structure can be interpreted in terms of the spatial distribution of the neutral gas with respect to the continuum sources that illuminate them. The narrow line component can be considered as result of gas in large-scale galactic features, such as has been suggested to explain a similar HI absorption feature in the ULIRG Mrk 273 (Cole et al. 1999). The slight velocity gradient observed in the narrow line component, approximately N-S in direction, suggests some global motion of this large-scale gas. The broad absorption against N1 and S shows a larger velocity difference with a gradient of $\sim 99\,\mathrm{km\,s^{-1}\,arcsec^{-1}}$ compared to the smaller velocity gradient observed in the narrow absorption feature. This is consistent with bulk movement of a disc of neutral gas orientated with a position angle similar to that of the two cores. This assertion is supported by CO spectral line studies by Tacconi et al. (1999) which have found a highly disturbed thick disc-like structure lying between the two nuclei. Assuming the neutral CO and HI gas co-exist in this disc feature we would expect to see broad HI absorption against S and N1 with, to a lesser degree, some broad absorption against M but no broad absorption against N2. This is in fact what is seen, with the weaker continuum flux density of M producing subsequently weaker absorption.

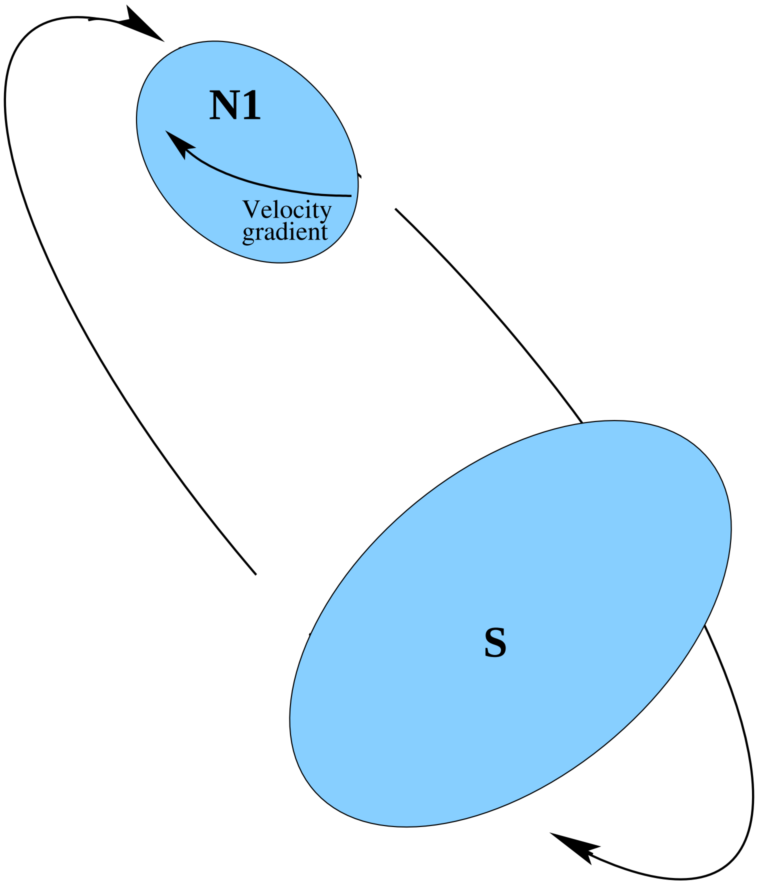

Figure 5.9: Schematic representation of the kinematics of NGC 6240.

5.7 Conclusions

Using MERLIN at 1.4 GHz, neutral hydrogen absorption has been imaged against the spatially extended background radio continuum source of NGC 6240. This has been used to determine distribution and kinematics of the neutral hydrogen in the central kiloparsec of this infrared merger at the highest angular resolution to date. High angular resolution radio continuum imaging of this central region at 1.4 GHz ($\sim0\farcs2$) and 5 GHz ($\sim0\farcs1$) have also been presented. The continuum images produced at 1.4 GHz and 5 GHz show a radio structure consistent with previous observations at a variety of wavelengths from 1.4 to 15 GHz (Colbert et al. 1994; Carral et al. 1990). The two brightest components, widely accepted as the remnant nuclei of the merging galaxies, are detected at both 1.4 and 5 GHz; they are observed as bright unresolved components separated by 1$''$.52 at 5 GHz. These two components display spectral indices of ∼0.7. Spectral indices cannot be used as evidence for or against the presence of AGNs in either or both of them. In this chapter I have also considered the possibility that the radio luminosity of this galaxy originates from either densely spaced regions of luminous radio supernovae or a pair of AGN situated in the remnant nuclei of the merging galaxies . Using energy and radio structure considerations, it is likely that the radio emission is the result of a combination of these two power sources and this conclusion is used to try to explain the extended continuum structure observed in the lower resolution 1.4 GHz maps. These conclusions have been vindicated by a recent observation of a luminous RSN within the central region of NGC 6240 and from modelling of the spectral energy distribution (SED) by (Lira et al. 2002) who find it necessary to include both AGN and starburst components to account for the observed X-ray characteristics.

Broad HI absorption is observed against these two nuclei, with a velocity difference of 150 km s^{-1}. These velocity characteristics can be explained by neutral gas sitting in a disc-like structure aligned along the position angle of the two nuclei such as is observed for CO gas by Tacconi et al. (1999). An alternative explanation is that the gas responsible for the broad absorption is associated with each remnant nuclei and that these are orbiting each other (see Fig. 5.8). This also explains the differences in velocity structures seen against N1 and S; N1 shows a clear velocity gradient whereas S shows broad absorption but with no distinct velocity gradient (see Fig. 5.7). Following this interpretation NGC 6240 shows considerable similarity to Arp 220. From MERLIN HI absorption observations, Mundell et al. (2001) proposed that Arp 220 consists of two counter-rotating discs associated with the remnant merger nuclei.

The velocity difference of 150 km s^{-1} is comparable with Tacconi et al's CO observations and recent stellar CO absorption data (Tecza et al. 2000). In addition, a narrow absorption component is observed superimposed upon this broad absorption. This is observed against the two nuclei and also against a weaker continuum features N2 and M where little or no broad absorption is seen. This narrow component can be interpreted as absorption by quiescent neutral gas in the outer parts of the merger. The velocity structure of this merging system is clearly much more complex than the simple interpretations considered here but these results, in conjunction with other evidence, point towards a disc-like neutral gas structure formed between the two merging galaxy nuclei.